Atomic structure of embedded Fe nanoclusters as a function of host matrix material: a synchrotron radiation study

2004 J. Phys.: Condens. Matter 16 7813

(http://iopscience.iop.org/0953-8984/16/43/020)

INSTITUTE OF PHYSICS PUBLISHING JOURNAL OF PHYSICS: CONDENSED MATTER

J. Phys.: Condens. Matter **16** (2004) 7813–7821 PII: S0953-8984(04)81645-X

Atomic structure of embedded Fe nanoclusters as a function of host matrix material: a synchrotron radiation study

S H Baker[1,3], M Roy[1], S J Gurman[1], S Louch[1], A Bleloch[2] and C Binns[1]

[1] Department of Physics and Astronomy, University of Leicester, Leicester LE1 7RH, UK
[2] Daresbury Laboratory, Daresbury, Warrington, Cheshire WA4 4AD, UK

E-mail: bak@le.ac.uk

Received 3 June 2004
Published 15 October 2004
Online at stacks.iop.org/JPhysCM/16/7813
doi:10.1088/0953-8984/16/43/020

Abstract

The atomic structure of Fe nanoclusters embedded in a range of matrix materials has been studied using synchrotron radiation. In particular, the effect of embedding the clusters in Ag, amorphous carbon (a-C) and a porous C_{60} matrix is investigated. The embedded cluster samples were prepared by co-deposition using a gas aggregation cluster source. Samples with both dilute and high-volume-filling fraction of clusters, at 4 and 40% respectively, were prepared. Fe K edge EXAFS measurements were used to probe the structure within the clusters. In a Ag matrix, the Fe clusters retain the b.c.c. structure of bulk Fe while in a-C there is evidence for both b.c.c. and f.c.c. structures in the clusters. These results are independent of cluster volume-filling fraction over the range investigated. When embedded in a porous C_{60} matrix, the Fe clusters oxidize to Fe_2O_3.

1. Introduction

Novel properties of magnetic nanoclusters, which include enhanced atomic orbital and spin moments [1, 2], have led to much recent research effort to develop 'new' magnetic materials assembled from nanoclusters. These include materials in which magnetic nanoclusters are embedded in a matrix of another material. A convenient method of preparing cluster-assembled materials directly is by co-deposition, using a molecular beam of the matrix material together with an intense size-selected cluster beam. This allows independent control of the cluster size and volume-filling fraction, leading to significant flexibility in the production of new magnetic materials. Potential applications include magnetic recording and storage.

[3] Author to whom any correspondence should be addressed.

The novel behaviour of magnetic nanoclusters arises in part from the high proportion of surface atoms with a reduced coordination; this causes a narrowing of the valence d bands and an increase in the density of states at the Fermi level. Both these effects enhance the spin magnetic moment towards the high-spin atomic limit [3, 4]. In addition, the orbital magnetic moment is increased due to spin–orbit coupling and the reduced symmetry in a cluster, which leads to a less effective quenching of the orbital magnetism by the crystal field. Further novel behaviour arises from the quantum size effect [5, 6] and modified electron screening behaviour.

Scanning probe techniques such as scanning tunnelling microscopy (STM) and atomic force microscopy (AFM) are now frequently used to image the morphology of clusters deposited on surfaces. There have been fewer investigations into the atomic structure within the clusters by e.g. using x-ray techniques, although several authors have used extended x-ray absorption fine structure (EXAFS) experiments to probe cluster structure. For example, Fe K edge EXAFS measurements in granular Fe/Cu films have shown that for Fe concentrations less than 22 at.% the structure of Fe clusters is face centred cubic (f.c.c.) while above 35 at.% Fe it reverts to the bulk body centred cubic (b.c.c.) structure [7]. Columnar-like nanoscale Fe islands, grown on N_2-dosed Cu(100), have been found to adopt a distorted f.c.c. structure [8]. Co K edge EXAFS experiments on melt-spun $Co_{10}Cu_{90}$ [9] and $Co_{15}Cu_{85}$ [10] ribbons indicate the formation of f.c.c. Co granules. In mixed Co–Ag clusters a core shell structure, in which a Ag shell surrounds the Co core, is expected due to the immiscibility between Co and Ag. However, Co edge EXAFS measurements on Co–Ag clusters embedded in MgO indicate that the Ag shell is not perfect with some Co atoms directly in contact with the matrix atoms [11]. The structure of Au clusters, stabilized by ligands of various types [12, 13], has been probed using Au L edge EXAFS and found to be f.c.c., as in bulk Au.

The atomic structure adopted by the clusters is expected to play a key role in determining their electronic and magnetic properties. This is true for ultra-thin Fe films, where the structure changes from b.c.c. to a distorted f.c.c. [14]; measured changes in magnetic moment using x-ray magnetic circular dichroism (XMCD) correlate with structural changes in the films [15]. In the case of magnetic clusters assembled within a matrix material, which may also affect the structure in the clusters, a knowledge of the intra-cluster structure is therefore important.

In this paper, we present the results of EXAFS experiments which were carried out in order to determine the atomic structure of Fe clusters embedded in a range of materials. These include Ag, amorphous carbon (a-C) and also a porous C_{60} matrix.

2. Experimental details

The embedded cluster films were prepared by co-deposition onto Si(100) substrates using a gas aggregation cluster source [16] and a molecular beam epitaxy (MBE) source (in the case of a Ag or C_{60} matrix) or a sputter source (in the case of an a-C matrix). Deposition rates of the Fe clusters and matrix material at the substrate were measured using a quartz crystal thickness monitor; this allowed us to set the volume-filling fraction (VFF) of clusters within the film by choosing the deposition rates appropriately.

The cluster source, described in detail elsewhere [16], is ultra-high-vacuum-compatible. Contaminant partial pressures of CO and H_2O during deposition were less than 4×10^{-10} mbar, and the base pressure in the deposition chamber was 2×10^{-10} mbar. The source produces a log-normal distribution of cluster sizes, with a most probable cluster size of $\sim$2 nm. A quadrupole filter, mounted axially in the source, allowed *in situ* measurement of the size distribution of deposited clusters (shown in figure 1). In all cases, a 250 Å buffer and 500 Å capping layer of the matrix material were deposited in order to help protect the cluster film against oxidation

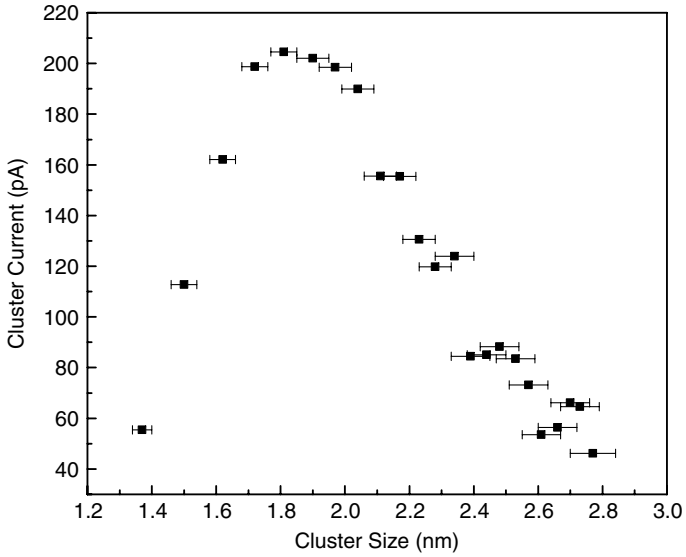

Figure 1. Size distribution of Fe cluters typically produced in the gas aggregation source, measured with the quadrupole filter operating at a size resolution of ±2.5% (mass resolution ±7.5%).

after removal from the deposition chamber. For the purposes of comparison, a 500 Å Fe film was also grown from an MBE source.

The atomic structure within the Fe clusters was probed by means of Fe K edge EXAFS experiments, carried out at the Synchrotron Radiation Source at Daresbury Laboratory. Except for the C_{60}-embedded samples, the measurements were performed on beamline 7.1 which has a double-crystal Si(111) monochromator. Harmonic rejection was set at 70% by detuning the monochromator and the incident x-ray intensity was measured by means of an ionization chamber containing an Ar/He gas mixture. The Fe edge absorption spectra $\mu(E)$ were measured using a nine-element monolithic Ge detector. Measurements for the C_{60}-embedded samples were made on beamline 9.2 at Daresbury, where the experimental set-up was similar except that harmonic rejection was set at 50% and the Fe edge spectra were recorded using a Canberra 13-element solid-state detector.

The measured absorption spectra $\mu(E)$ were background-subtracted and normalized using the Daresbury program EXBACK, which fits low-order polynomials to the smoothly varying background absorption. This yields the EXAFS spectra $\chi(E)$. These were then analysed to provide experimental values for structural parameters such as the bond lengths r_j, the mean square variations in bond length σ_j^2 (Debye–Waller factor) and coordination numbers N_j by fitting the experimental $\chi(E)$ to calculated EXAFS functions. This was achieved by means of the program EXCURV98 [17], which uses Hedin–Lundqvist potentials to calculate the scattering phase-shifts and employs the fast curved-wave theory of Gurman *et al* [18] to calculate $\chi(E)$. All errors are quoted to ±2 standard deviations.

3. Results and discussion

3.1. Fe/Ag

Figure 2 shows the EXAFS χ (weighted by k^3) and the associated Fourier transform for the Fe film grown by MBE; k is the photoelectron wavevector. A good fit to the data, entirely consistent

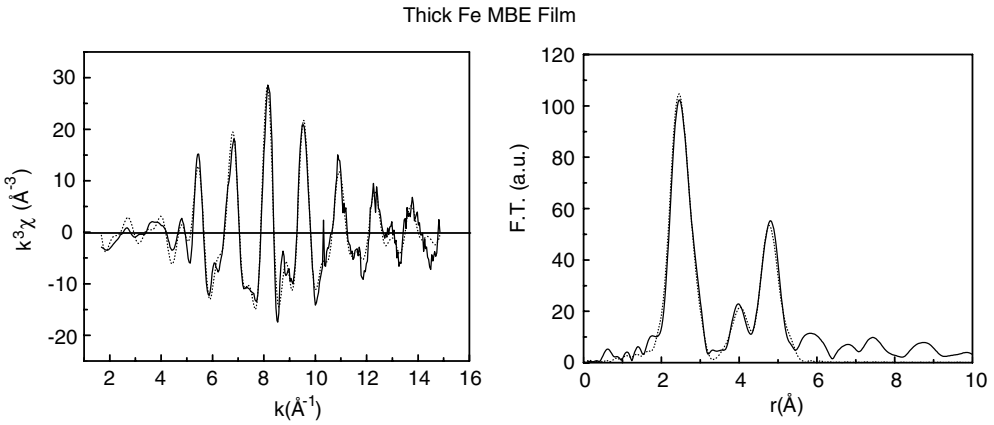

Figure 2. EXAFS spectrum χ (weighted by k^3) plotted as a function of photoelectron wavevector k, and associated Fourier transform (FT), for thick Fe film grown by MBE.

with b.c.c. Fe was obtained, with five statistically significant shells. The analysis program [17] allows multiple scattering effects to be included. In the fit here, we allowed for multiple scattering between shells 1 and 5 (expected in b.c.c. structures). The coordination numbers N_j were held fixed at the values associated with the b.c.c. structure, while the interatomic distances r_j and Debye–Waller factors $2\sigma_j^2$ were allowed to vary in the fit. Table 1 gives the fit parameters obtained; it is clear that they are consistent with b.c.c. Fe, as expected for a thick Fe film.

In figure 3, data for a sample containing 5% VFF of Fe clusters in Ag are presented. Initial inspection reveals that χ and the associated Fourier transform are similar to those obtained for the thick Fe film. This is confirmed in the analysis for which fits with four statistically significant shells were obtained. As the fit parameters in table 1 indicate, the data are consistent with b.c.c. Fe. Very similar results were obtained for a sample with 40% VFF of Fe. For such a high VFF, the clusters are expected to have percolated; since the clusters adopt the bulk Fe structure in the dilute case, we would not expect any change upon percolation. In principle, the coordinations N_j for small clusters should be decreased relative to the values for the corresponding bulk material; the amount by which they are reduced should allow one to estimate the cluster size and also (for a given crystal structure) cluster shape, e.g. icosahedral, cuboctahedral, etc. In the case of ligand-stabilized Au clusters, a number of authors have used EXAFS measurements in order to investigate the cluster shape [12, 13]. However, the magnitude of experimental uncertainties in N_j usually makes it difficult to draw exact conclusions about cluster shapes. Some of the experimental values of N_j in table 1 (in particular the first shell coordinations) hint at a size-related reduction, although in general the bulk values of N_j are included within the experimental uncertainties.

Including an Fe–Ag shell in the fits yielded an Fe–Ag distance of 2.81 ± 0.03 Å for both 5 and 40% VFF, together with an Fe–Ag coordination of 3.6 ± 2.6, although the improvements to the fits were small and possibly not statistically significant. However, the Fe–Ag coordination obtained is at least consistent with the cluster sizes present (see figure 1), for which up to $\sim$50% of the atoms are at the cluster surfaces.

It can be noted that the Debye–Waller factors tend to increase with increasing shell radius. This can be interpreted as being due to correlations in the thermal motions of the near neighbours [19].

Table 1. Structural parameters $r_j, N_j, 2\sigma_j^2$ (interatomic distance, coordination, Debye–Waller factor, respectively) obtained from fits to the EXAFS for films of Fe clusters embedded in Ag, and also an Fe MBE film. Figures for N_j in parentheses indicate that they were held fixed at these values during the fits. Also included are the interatomic distances and coordinations in bulk b.c.c. Fe.

Sample	r (Å)	N	$2\sigma^2$ (Å^2)
		Shell 1	
Fe MBE Film	2.49 ± 0.01	(8)	0.012 ± 0.001
5% VFF Fe in Ag	2.49 ± 0.01	6.2 ± 0.4	0.013 ± 0.001
40% VFF Fe in Ag	2.49 ± 0.01	5.6 ± 0.6	0.013 ± 0.001
B.C.C. Fe	2.49	8	
		Shell 2	
Fe MBE Film	2.84 ± 0.01	(6)	0.023 ± 0.003
5% VFF Fe in Ag	2.85 ± 0.01	7.8 ± 2.5	0.040 ± 0.010
40% VFF Fe in Ag	2.85 ± 0.01	8.4 ± 3.9	0.039 ± 0.010
B.C.C. Fe	2.87	6	
		Shell 3	
Fe MBE Film	4.09 ± 0.01	(12)	0.022 ± 0.003
5% VFF Fe in Ag	4.10 ± 0.01	14.0 ± 4.5	0.039 ± 0.010
40% VFF Fe in Ag	4.08 ± 0.02	5.6 ± 3.0	0.021 ± 0.010
B.C.C. Fe	4.06	12	
		Shell 4	
Fe MBE Film	4.80 ± 0.01	(24)	0.014 ± 0.001
5% VFF Fe in Ag	4.79 ± 0.01	22.3 ± 4.3	0.026 ± 0.004
40% VFF Fe in Ag	4.77 ± 0.01	21.2 ± 5.6	0.024 ± 0.005
B.C.C. Fe	4.76	24	
		Shell 5	
Fe MBE Film	5.19 ± 0.04	(8)	0.024 ± 0.001
5% VFF Fe in Ag			
40% VFF Fe in Ag			
B.C.C. Fe	4.97	8	

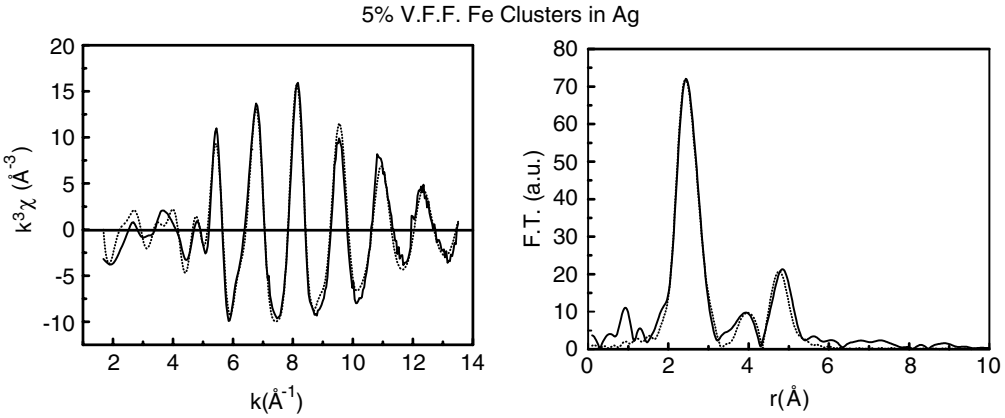

Figure 3. EXAFS spectrum $k^3\chi$ and associated Fourier transform for a sample containing 5% VFF of Fe clusters embedded in a Ag matrix.

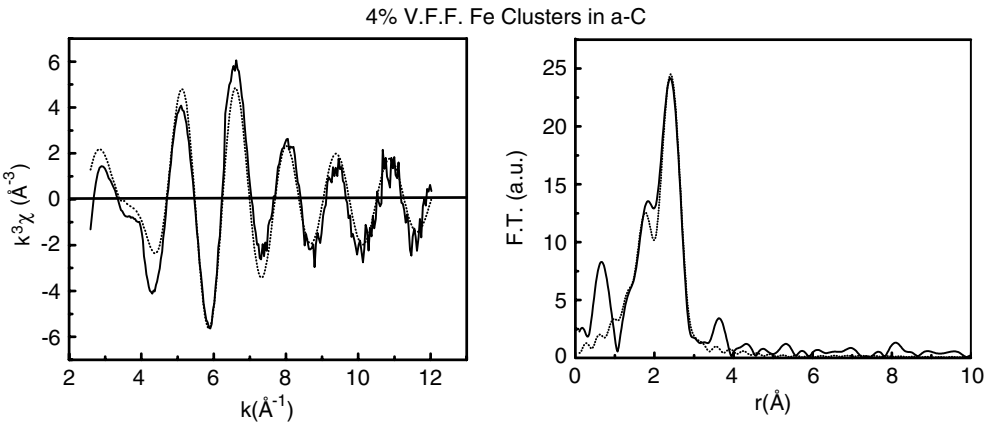

Figure 4. EXAFS spectrum $k^3\chi$ and associated Fourier transform for a sample containing 4% VFF of Fe clusters in an a-C matrix.

Table 2. Structural parameters $r_j, N_j, 2\sigma_j^2$ (interatomic distance, coordination, Debye–Waller factor, respectively) obtained from fits to the EXAFS for films of Fe clusters embedded in a-C.

Sample	r (Å)	N	$2\sigma^2$ (Å^2)
		Shell 1, Fe–O	
4% VFF Fe in a-C	1.92 ± 0.02	1.2 ± 0.2	0.013 ± 0.005
40% VFF Fe in a-C	1.95 ± 0.02	1.9 ± 0.3	0.016 ± 0.004
		Shell 2, Fe–Fe	
4% VFF Fe in a-C	2.49 ± 0.01	1.0 ± 0.3	0.010 ± 0.004
40% VFF Fe in a-C	2.46 ± 0.01	0.5 ± 0.1	0.002 ± 0.003
		Shell 3, Fe–Fe	
4% VFF Fe in a-C	2.56 ± 0.02	4.2 ± 1.3	0.037 ± 0.007
40% VFF Fe in a-C	2.57 ± 0.01	3.2 ± 0.6	0.023 ± 0.004

3.2. Fe/a-C

For the a-C embedded samples, both $k^3\chi$ and their Fourier transforms are different in appearance from those presented earlier. Data for a sample containing 4% VFF of Fe clusters in an a-C matrix are shown in figure 4. The shoulder in the Fourier transform at less than 2.0 Å is indicative of partial oxidation. As the fit parameters listed in table 2 show, it is possible to account for this in the fits which yield an Fe–O separation of 1.92 ± 0.02 Å. This is in good agreement with the Fe–O nearest-neighbour distances in Fe_2O_3 of 1.95 Å. High-resolution transmission electron microscope (TEM) images provide more information on the extent of oxidation in the sample. Figure 5 shows a TEM image, recorded using the SuperSTEM at Daresbury Laboratory, of an Fe cluster/a-C thin film deposited directly onto a Cu TEM grid and prepared under identical conditions to the samples studied in the EXAFS experiments. The TEM image reveals the presence of holes or voids in the a-C matrix—indicated by the dark area in the image. We suggest that the density of these is great enough in places for air pores to penetrate from the capping layer into the bulk of the film i.e. the film is partially porous. Hence oxidation is confined to Fe clusters situated in the voids or pores in the a-C film, but away from these the clusters are properly encapsulated and well protected.

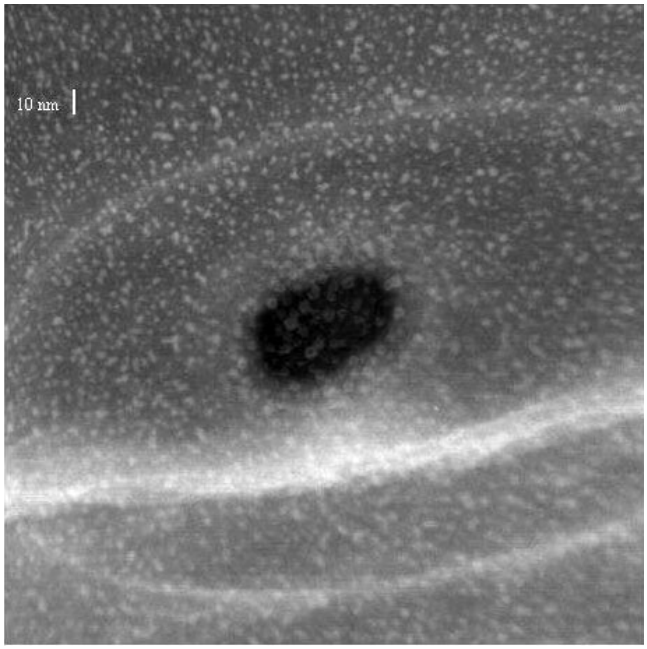

Figure 5. High resolution TEM image of a film of Fe clusters embedded in a-C. The dark area in the image indicates the presence of a hole in the a-C matrix; individual clusters, which appear as bright spots, are evident throughout the sample.

The important result from the fitting to the spectra from the a-C embedded samples comes from the Fe–Fe nearest-neighbour separations. For samples with VFF of 4 and 40%, the fits yield first- and second-nearest-neighbour Fe–Fe distances of 2.47 ± 0.02 and 2.57 ± 0.02 Å. These values are in good agreement with the first nearest-neighbour distances in both b.c.c. Fe (2.49 Å) and f.c.c. Fe (2.57 Å), indicating that both structures are present. It should be noted that the shortest Fe–Fe interatomic distances in Fe_2O_3 and FeO, 2.97 and 3.03 Å, respectively, are considerably larger.

The coordinations can be used to estimate the proportions of the two structures present. An Fe–O coordination of 3 is expected at 1.95 Å in Fe_2O_3 (see table 3). Hence, the Fe–O coordination of 1.2 ± 0.2 in the 4% VFF sample implies an oxide content in the range 33–47%. With nearest-neighbour coordinations of 12 and 8 in the f.c.c. and b.c.c. structures, respectively, the measured coordinations of 4.2 ± 1.3 (for f.c.c.) and 1.0 ± 0.3 (for b.c.c.) in the same sample are consistent with 37–45% f.c.c. Fe and 8–16% b.c.c. Fe. For the 40% VFF sample, the corresponding figures are 22–32% f.c.c. Fe and 5–7% b.c.c. Fe with an oxide content in the range 53–73%. Since we would expect that the clusters are percolated in this case, the proportion of b.c.c. (bulk structured) Fe should be expected to be larger than in the dilute sample. The size of our experimental errors, however, is such that this effect is masked in our data.

Attempts to include an Fe–C shell in the fits provided only very small improvements which were not really significant. However, the Fe–C distance obtained in such fits of 1.82 ± 0.02 Å (with an Fe–C coordination of 0.5 ± 0.2) is at least consistent within error with the value of 1.84 ± 0.02 Å obtained for f.c.c. Fe films on C(100) [20]. It is also consistent with the reported minimum Fe–C distance in FeC solid solutions [21].

Table 3. Interatomic distances and coordinations in FeO and Fe_2O_3, as well as the structural parameters $r_j, N_j, 2\sigma_j^2$, obtained from fits to the EXAFS for a film containing 8% VFF of Fe clusters in C_{60}.

Sample	Atom type	r (Å)	N	$2\sigma^2$ (Å^2)
		Shell 1		
FeO structure	O	2.15	6	
Fe_2O_3 structure	O	1.95	3	
8% VFF Fe in C_{60}	O	1.96 ± 0.01	(3)	0.010 ± 0.002
		Shell 2		
FeO structure	Fe	3.04	12	
Fe_2O_3 structure	O	2.12	3	
8% VFF Fe in C_{60}	O	2.06 ± 0.03	(3)	0.039 ± 0.008
		Shell 3		
FeO structure	O	3.73	8	
Fe_2O_3 structure	Fe	2.97	4	
8% VFF Fe in C_{60}	Fe	3.04 ± 0.02	(4)	0.031 ± 0.004
		Shell 4		
FeO structure	Fe	4.30	6	
Fe_2O_3 structure	Fe	3.36	3	
8% VFF Fe in C_{60}	Fe	3.50 ± 0.05	(3)	0.032 ± 0.013

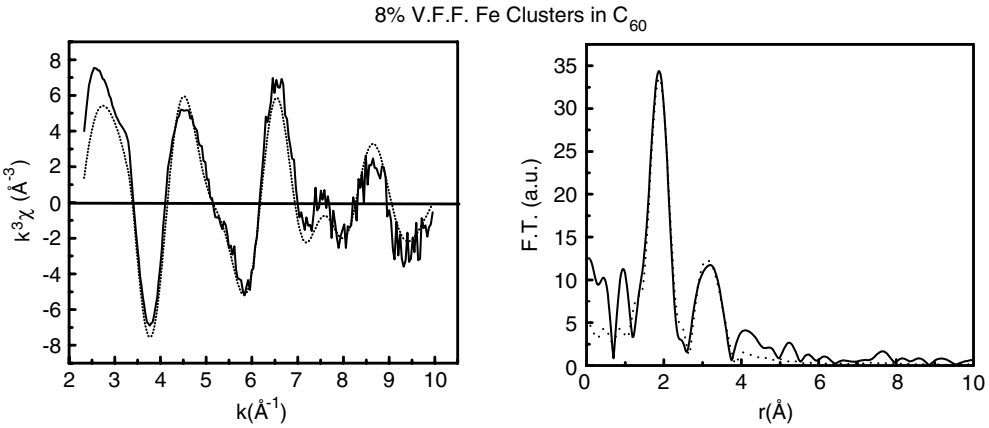

Figure 6. EXAFS spectrum $k^3\chi$ and associated Fourier transform for a sample containing 8% VFF of Fe clusters in a C_{60} matrix.

3.3. Fe/C60

Figure 6 presents $k^3\chi$ and its Fourier transform for a sample containing 8% VFF of Fe clusters embedded in a C_{60} matrix. Given the porous nature of the C_{60} matrix, it is not surprising that the Fe clusters are heavily oxidized; a thick capping layer of C_{60} is not sufficient to protect against oxidation in this case. Table 3 gives the coordinations and interatomic distances for the Fe_2O_3 and FeO structures. Constrained fits were applied, in which N_j were held at the values listed in table 3 with r_j and σ_j^2 allowed to vary. Fitting to the Fe_2O_3 structure proved significantly more successful than to FeO. The fit parameters obtained for the Fe_2O_3 fit are given in table 3.

4. Summary

The atomic structure of embedded Fe nanoclusters is strongly influenced by the nature of the host matrix material. In Ag, the clusters retain the b.c.c. structure of bulk Fe down to a concentration of 4% VFF. In an a-C matrix, there is evidence for both b.c.c. and f.c.c. structures in the Fe nanoclusters. This is true at both dilute and higher cluster concentrations. When the Fe clusters are embedded in a porous C_{60} matrix, the clusters oxidize to Fe_2O_3.

Acknowledgments

The authors are grateful for the assistance of Mr R L Bilsborrow and Dr J F W Mosselmans at Daresbury Laboratory during the collection of the EXAFS data. We are also grateful for support from EC contract number G5RD-CT-2001-00478 (AMMARE).

References

[1] Edmonds K W, Binns C, Baker S H, Thornton S C, Norris C, Goedkoop J B, Finazzi M and Brookes N B 1999 *Phys. Rev.* B **60** 472
[2] Baker S H, Binns C, Edmonds K W, Maher M J, Thornton S C, Louch S and Dhesi S S 2002 *J. Magn. Magn. Mater.* **247** 19
[3] Billas I M L, Becker J A, Chtelain A and de Heer W A 1993 *Phys. Rev. Lett.* **71** 4067
[4] Douglass D C, Cox A J, Bucher J P and Bloomfield L A 1993 *Phys. Rev.* B **47** 12874
[5] Koboyashi S, Takahasi T and Sasaki J 1972 *J. Phys. Soc. Japan* **32** 1234
[6] Kubo R 1962 *J. Phys. Soc. Japan* **17** 975
[7] Sakurai M, Makhlouf S A, Hihara T, Sumiyama K, Wakoh K and Suzuki K 1995 *Physica* B **208&209** 614
[8] Finetti P, Dhanak V R, Binns C, Edmonds K W, Baker S H and D'Addato S 2001 *J. Electron Spectrosc. Relat. Phenom.* **114–116** 251
[9] Vergara M P C, Cezar J C, Tolentino H C N and Knobel M 2002 *Physica* B **320** 143
[10] Prieto A G, Fdez-Gubieda M L, Garcia-Arribas A, Barandiaran J M, Meneghini C and Mobilio S 2000 *J. Magn. Magn. Mater.* **221** 80
[11] Favre L, Stanescu S, Dupusi V, Bernstein E, Epicier T, Melinon P and Perez A 2004 *Appl. Surf. Sci* **226** 265
[12] Cluskey P D, Newport R J, Benfield R E, Gurman S J and Schmid G 1993 *Z. Physik* D **26** S8–S11
[13] Benfield R E, Grandjean D, Kroll M, Pugin R, Sawitowski T and Schmid G 2001 *J. Phys. Chem.* B **105** 1961
[14] Heinz K, Bayer P and Muller S 1995 *Surf. Rev. Lett.* **2** 89
[15] Ohresser P, Brookes N B, Padovani S, Scheurer F and Bulou H 2001 *Phys. Rev.* B **64** 104429
[16] Baker S H, Thornton S C, Edmonds K W, Maher M J, Norris C and Binns C 2000 *Rev. Sci. Instrum.* **71** 3178
[17] Binsted N 1998 EXCURV98: CCLRC Daresbury Laboratory computer program
[18] Gurman S J, Binsted N and Ross I 1984 *J. Phys. C: Solid State Phys.* **17** 143
[19] Gurman S J and Pendry J B 1976 *Solid State Commun.* **20** 287
[20] Swineford R S, Pappas D P and Harris V G 1995 *Phys. Rev.* B **52** 7890
[21] *International Tables of X-ray Crystallography* 1962 (Birmingham, England: International Union of Crystallography)